

Quantum Rotor Atoms in Light Beams with Orbital Angular Momentum: Highly Accurate Rotation Sensor

Igor Kuzmenko^{1,2,4}, Tetyana Kuzmenko^{1,4}, Y. B. Band^{1,2,3,4}

¹Department of Physics, Ben-Gurion University of the Negev, Beer-Sheva 84105, Israel

²Department of Chemistry, Ben-Gurion University of the Negev, Beer-Sheva 84105, Israel

³Department of Electro-Optics, Ben-Gurion University of the Negev, Beer-Sheva 84105, Israel

⁴The Ilse Katz Center for Nano-Science, Ben-Gurion University of the Negev, Beer-Sheva 84105, Israel

Atoms trapped in a red detuned retro-reflected Laguerre-Gaussian beam undergo orbital motion within rings whose centers are on the axis of the laser beam. We determine the wave functions, energies and degeneracies of such quantum rotors (QRs), and the microwave transitions between the energy levels are elucidated. We then show how such QR atoms can be used as high-accuracy rotation sensors when the rings are singly-occupied.

PACS numbers: 32.80.Pj, 71.70.Ej, 73.22.Dj

Introduction: We show that quantum rotor (QR) atoms (atoms whose motion is constrained to a circular ring) [1] can be formed in light beams having orbital angular momentum and that they can be used as an extremely high accuracy rotation sensor. QR atoms are trapped in a red-detuned linearly polarized retro-reflected Laguerre-Gaussian (LG) beam [2–6]. A line of singly-occupied rings filled with QR atoms can be easily formed (see Fig. 1) [7–9]. Single-occupation and negligible tunneling between rings are important to suppress deleterious spin exchange collisions between QR atoms for sensor applications. The accuracy obtained here suggests that this can be the highest precision rotation sensor proposed so far in the literature.

A LG beam propagating along the z -axis with orbital angular momentum l and polarization \mathbf{e}_α can be written in terms of a slowly varying envelope $u_{l,p}(r, \phi, z)$ of the electric field as

$$\mathbf{E}_{\alpha,l,p}(\mathbf{r}, t) = u_{l,p}(r, \phi, z) e^{i(kz - kz_0 - \omega t)} \mathbf{e}_\alpha + \text{c.c.}, \quad (1)$$

with field amplitude mode $LG_p^l(\mathbf{r}) \equiv u_{l,p}(\mathbf{r})$ [2–4],

$$\begin{aligned} u_{l,p}(r, \phi, z) = & \sqrt{\frac{2p!}{\pi(p+|l|)!}} \frac{\sqrt{P_0/c}}{w(z)} \left(\frac{r\sqrt{2}}{w(z)} \right)^{|l|} \exp\left(-\frac{r^2}{w^2(z)}\right) \\ & \times L_p^{|l|} \left(\frac{2r^2}{w^2(z)} \right) \exp\left(-\frac{ikr^2z}{2(z^2+z_R^2)}\right) \exp(-il\phi) \\ & \times \exp\left[i(2p+|l|+1)\tan^{-1}\left(\frac{z}{z_R}\right)\right]. \end{aligned} \quad (2)$$

Here z is the longitudinal distance from the beam waist located at $z = 0$, P_0 is the laser beam power, w_0 is the beam waist at $z = 0$, $R(z) = z(1 + (z/z_R)^2)$ is the radius of curvature of the beam wavefront, $w(z) = w_0(1 + (z/z_R)^2)^{1/2}$ is the radius at which the beam intensity falls to $1/e$ of its axis value at z , $z_R = \pi w_0^2/\lambda$ is the Rayleigh range for the laser with wavelength $\lambda = 2\pi/k$ where $k = \omega/c$ is the wavenumber, $0 < z_0 < \lambda/2$ is a phase parameter, $L_p^{|l|}(x)$ is the associated Laguerre polynomial, ϕ is the azimuthal angle, and $\tan^{-1}(z/z_R)$ is the Gouy phase. Figure 1(a) is a schematic diagram of a retro-reflected LG beam propagating along the z -axis, and Fig. 1(b) shows superposition of two counter-propagating beams that form a

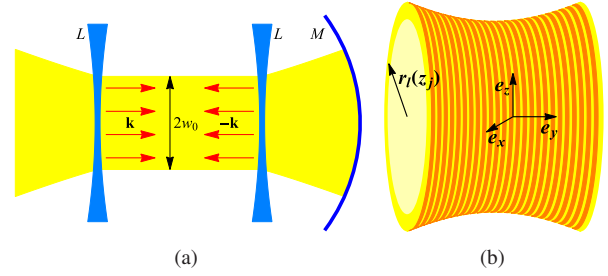


FIG. 1: (a) Two lenses (L) refract the LG beam (yellow region). The mirror (M) reflects the beam, and two counter-propagating beams result. An almost uniform beam waist w_0 between the lenses, and a series of ring optical potentials with zero amplitude at the center are stacked perpendicular to the beam axis. The wave vectors of the incident and reflected beams are $\pm\mathbf{k}$. (b) Blowup of the region between the two mirrors where the LG beam forms the ring shaped potential wells. Yellow and orange denote potential minima and maxima. \mathbf{e}_x , \mathbf{e}_y and \mathbf{e}_z are unit vectors parallel to the x , y and z -axes, and $(r_l(z_j), z_j)$ are minima of the potential energy.

standing wave along the z -axis. The slowly varying envelope $u_{l,p}(r, \phi, z)$ of the counter-propagating (cp) standing wave has the form

$$\mathbf{E}_{\alpha,l,p}^{\text{cp}}(\mathbf{r}, t) = u_{l,p}(r, \phi, z) \mathbf{e}_\alpha (e^{i(kz - kz_0 - \omega t)} + e^{i(-kz + kz_0 - \omega t)}). \quad (3)$$

This standing wave configuration results in a series of ring shaped optical potentials [see the orange rings in Fig. 1(b)] stacked perpendicular to the axis of the beams. Since our interest is in trapping atoms in the light beam, the light is red-detuned from atomic resonance, and atoms will be trapped in the ring shaped optical potentials that are singly occupied so that spin relaxation collisions are suppressed [10].

QR Bound States in LG Rings: The QR Hamiltonian operator in cylindrical coordinates is

$$H = -\frac{\hbar^2}{2M} \left(\frac{\partial^2}{\partial r^2} + \frac{1}{r} \frac{\partial}{\partial r} + \frac{1}{r^2} \frac{\partial^2}{\partial \phi^2} + \frac{\partial^2}{\partial z^2} \right) + V(r, \phi, z), \quad (4)$$

where the first term is the atom kinetic energy in polar coordinates and $V(r, \phi, z)$ is the optical potential resulting from the LG beams, which is calculated as a second-order ac Stark

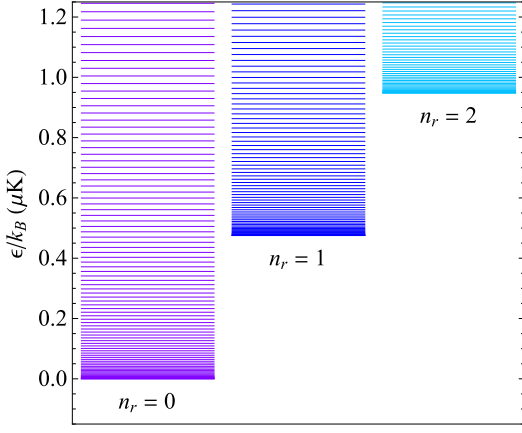


FIG. 2: Energies $\epsilon(n_z, n_r, m_\ell)$ of the QR (relative to the QR ground state energy) trapped in an LG beam with $w_0 = 10 \mu\text{m}$, $l = 5$, $p = 0$, and $V_0 = 10 \mathcal{E}_0$, where \mathcal{E}_0 is the recoil energy. This gives $r_l \equiv r_l(z_j)$ with $j = 0$ equal to $15.81 \mu\text{m}$. Energies with $n_r = 0$ are shown as purple lines, $n_r = 1$ as blue lines and $n_r = 2$ as sky-blue lines. Quantum states with $n_z \geq 1$ have very high energies and fall out of the scale of the figure, hence only $n_z = 0$ are shown.

shift [11] and is given in terms of the ac polarizability $\alpha(\omega)$ by $V(\mathbf{r}) = -\alpha(\omega)|\mathbf{E}_{\alpha,l,p}^{\text{cp}}(\mathbf{r}, t)|^2$. In the standing wave configuration in the nearly constant beam waist region, the optical potential can be taken to be two-dimensional since the width of the rings are very small. For a LG_0^l mode ($p = 0$ and $l \neq 0$), the potential is independent of ϕ ,

$$V(r, z) = -V_0 \cos^2(k(z - z_0)) \frac{\rho^{2|l|}(z)}{w^2(z)} e^{-|l|(\rho^2(z)-1)}, \quad (5)$$

where $\rho(z) = r/r_l(z)$ and $w(z) = w(z)/w_0$. Potential (5) has a minimum at

$$z = z_j \equiv \frac{\pi}{k} j + z_0, \quad r = r_l(z_j) \equiv w(z_j) \sqrt{|l|/2}, \quad (6)$$

where j is integer. The trapped atoms execute circular motion around the z axis, i.e., they are QRs. $V(r_l(z_j), z_j)$ is given by $V(r_l(z_j), z_j) = -V_0 (w_0/w(z_j))^2$. For z close to z_j ,

$$V(r, z) \approx V_l(r) + W_j(z), \quad (7)$$

where

$$V_l(r) = V(r, z_j), \quad W_j(z) = \frac{V_0 k^2}{w^2(z_j)} (z - z_j)^2. \quad (8)$$

$W_j(z)$ is a harmonic potential in $z - z_j$. The corresponding harmonic frequency and length are

$$\omega_z(z_j) = \frac{2}{w(z_j)} \frac{\sqrt{\mathcal{E}_0 V_0}}{\hbar}, \quad b_z(z_j) = \frac{\sqrt{w(z_j)}}{k} \left(\frac{\mathcal{E}_0}{V_0} \right)^{1/4}, \quad (9)$$

where $\mathcal{E}_0 = \hbar^2 k^2 / (2M)$ is the recoil energy.

The optical potential (5) is invariant with respect to rotations about the z axis, therefore the quantum states of the QR

in the harmonic approximation (7) are parametrized by radial and vertical quantum numbers n_r and n_z describing radial and z motion ($n_r, n_z = 0, 1, 2, \dots$), the orbital momentum quantum number m_ℓ and projection m_F of the hyperfine orbital momentum \mathbf{F} on the z axis. The ground state has $n_z = n_r = m_\ell = 0$, and is $2F + 1$ fold degenerate. Orbital excited states with $m_\ell \neq 0$ are $2(2F + 1)$ fold degenerate, and have angular momentum $\pm m_\ell$. Radial and vertical excitations have $n_r \neq 0$ and $n_z \neq 0$ respectively. For simplicity, in this paragraph, let us consider an atom trapped at the z_0 site (i.e., near z_j with $j = 0$). The QR wave functions and eigen-energies satisfy the Schrödinger equation,

$$\left[-\frac{\hbar^2}{2M} \nabla^2 + V(r, z) - \epsilon_{\mathbf{n}} \right] \Psi_{\mathbf{n}}(\mathbf{r}) = 0, \quad (10)$$

where $\mathbf{n} = (n_z, n_r, m_\ell)$. The wave function can be written in cylindrical coordinates $\mathbf{r} = (r, \phi, z)$ as

$$\Psi_{\mathbf{n}}(\mathbf{r}) = \frac{1}{\sqrt{2\pi}} \eta_{n_z}(z) \psi_{n_r, m_\ell}(r) e^{im_\ell \phi}, \quad (11)$$

where $\eta_{n_z}(z)$ and $\psi_{n_r, m_\ell}(r)$ satisfy the equations,

$$\left[-\frac{\hbar^2}{2M} \frac{d^2}{dz^2} + W_0(z) - \epsilon_z(n_z) \right] \eta_{n_z}(z) = 0, \quad (12)$$

$$\left[-\frac{\hbar^2}{2Mr} \frac{d}{dr} \left(r \frac{d}{dr} \right) + V_l(r) + m_\ell^2 C(r) - \epsilon_r(n_r, m_\ell) \right] \psi_{n_r, m_\ell}(r) = 0. \quad (13)$$

$V_l(r)$ and $W_j(z)$ are given by Eq. (8), and $C(r) = \frac{\hbar^2}{2Mr^2}$ is the rotational energy of the QR around the z axis. The eigen-energy of the trapped atom is

$$\epsilon(\mathbf{n}) = \epsilon_z(n_z) + \epsilon_r(n_r, m_\ell), \quad (14)$$

where $r_l \equiv r_l(z_j)$ with $j = 0$. The QR vertical, radial and orbital excitation energies are

$$\begin{aligned} \epsilon_z &= \epsilon_z(1) - \epsilon_z(0) \approx \hbar\omega_z, \\ \epsilon_r &= \epsilon_r(1, 0) - \epsilon_r(0, 0), \\ \epsilon_\ell &= \epsilon_r(0, 1) - \epsilon_r(0, 0) \approx C(r_l). \end{aligned}$$

We assume they satisfy the inequalities,

$$\epsilon_z \gg \epsilon_r \gg \epsilon_\ell, \quad (15)$$

i.e., the orbital excitations are the lowest-energy excitations, whereas the radial and longitudinal excitations have relatively high energies. The energies $\epsilon(n_z = 0, n_r, m_\ell)$, Eq. (14), are shown in Fig. 2. For $l = 5$, $w_0 = 10 \mu\text{m}$, $r_l = 15.81 \mu\text{m}$ and $V_0 = 10 \mathcal{E}_0 = k_B \times 35.36 \mu\text{K}$, the excitation energies are $C(r_l) = k_B \times 0.1613 \text{ nK}$, $\hbar\omega_r = k_B \times 0.4776 \mu\text{K}$ and $\hbar\omega_z = k_B \times 22.36 \mu\text{K}$, so the inequalities (15) are valid. Quantum states with $n_z \geq 1$ have high energies and are not shown in Fig. 2.

Rabi Oscillation Method with Raman Pulses: In order to measure the excitation energies of the QR atoms with quantum numbers n_r , m_ℓ and m_F , we propose to subject the QRs

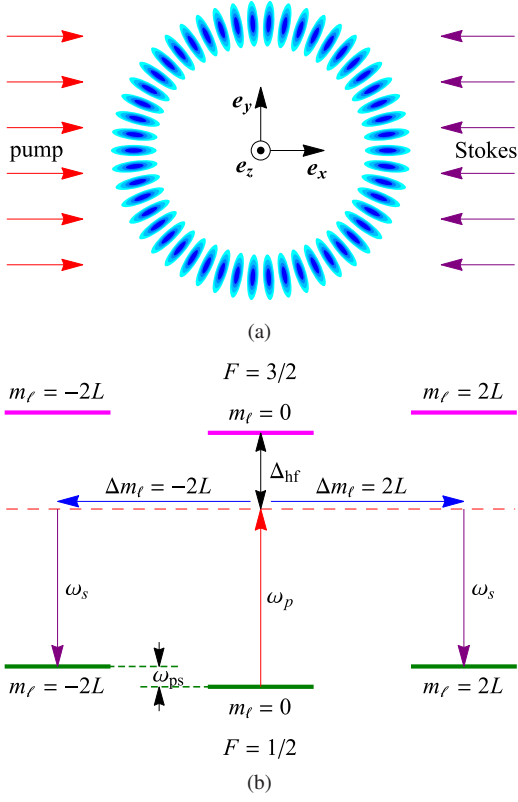


FIG. 3: (a) Pump and Stokes radio-frequency pulses (red and purple arrows) and optical rotational counter-propagating LG rotational-kick-pulses with $L = 25$ along the z axis. The blue regions indicate the depth of the rotational-kick optical pulse potential. \mathbf{e}_x , \mathbf{e}_y and \mathbf{e}_z are unit vectors along the x -, y - and z -axes. (b) Quantum transitions due to the pump, Stokes and rotational-kick pulses (red, purple and blue arrows). The frequencies of the pump and Stokes pulses are ω_p and ω_s , and their difference $\omega_{ps} = \omega_p - \omega_s$ is equal to the transition frequency $\omega_{2L,0}$. Detuning of ω_p from the resonant frequency of the ${}^2S_{1/2}(F = 1/2)$ to ${}^2S_{1/2}(F = 3/2)$ quantum transition is Δ_{hf} .

to three pulses, as shown in Fig. 3(a): pump and Stokes radio-frequency pulses with frequencies $\omega_p \gtrsim \omega_s$ that are detuned from the quantum transition between the hyperfine states of the ground state, and a LG pulse with frequency ω_e far-detuned from the resonant frequency of the ${}^2S_{1/2} \rightarrow {}^2P_{3/2}$ electronic transition. The radio-frequency pump and Stokes light cannot change the orbital quantum number m_ℓ . Therefore we use a LG pulse that allows quantum transitions $|m_\ell\rangle \rightarrow |m'_\ell\rangle$ between quantum states with different orbital quantum numbers m_ℓ and m'_ℓ [see Fig. 3(b)]. The pump and Stokes pulses propagate parallel and anti-parallel to the x -axis and are linearly polarized with magnetic field along the z axis (see the supplemental materials (SM) [14]). The pump and Stokes magnetic fields are given by $\mathbf{B}_\mu(\mathbf{r}, t) = \mathbf{B}_\mu^{(0)} \cos(k_\mu x - i\omega_\mu t)\Theta(t)\Theta(\tau - t) \approx \mathbf{B}_\mu^{(0)} \cos(\omega_\mu t)\Theta(t)\Theta(\tau - t)$, where $\mu = p, s$ (pump and Stokes beams) and we have assumed square pulses, hence the presence of the Θ functions. Here we take into account that the wavelengths λ_μ are much longer than the radius r_l of the QR, hence \mathbf{B}_μ depends on t , but not on \mathbf{r} , and

therefore these pulses do not possess Raman transitions between the quantum states $|n_r, m_\ell\rangle$ and $|n'_r, m'_\ell\rangle$ and we can approximate $\mathbf{B}_\mu(\mathbf{r}, t)$ by $\mathbf{B}_\mu(t) \equiv \mathbf{B}_\mu(0, t)$. Hence, the dipole magnetic interaction between the QR and the radio waves, $H_\mu = -g_F \mu_B \mathbf{F} \cdot \mathbf{B}_\mu(t)$, does not depend on \mathbf{r} (the position of the atom), and therefore $\langle n_r, m_\ell | H_\mu | n'_r, m'_\ell \rangle \propto \delta_{n_r, n'_r} \delta_{m_\ell, m'_\ell}$. For Raman transitions $|n_r, m_\ell\rangle \rightarrow |n'_r, m'_\ell\rangle$ with $m_\ell \neq m'_\ell$, an optical square pulse which breaks the cylindrical symmetry of the QR is required. The electric field of the optical pulse is $\mathbf{E}_e(\mathbf{r}, t) = \frac{1}{2}(u_{L,0}(\mathbf{r}) + u_{-L,0}(\mathbf{r})) \cos(k_e z) \Theta(t)\Theta(\tau - t) e^{-i\omega_e t} \mathbf{e}_x + \text{c.c.}$, where $k_e = \omega_e/c$ is the wavenumber of the optical pulse and $u_{L,0}(\mathbf{r})$ is given by Eq. (2). We choose the waist radii of the LG pulse w_e and the LG beam waist w_0 , and their orbital angular momentums L and l in such a way that $w_e \sqrt{|L|/2} = w_0 \sqrt{|l|/2}$.

The stimulated Raman process corresponding to absorption of a pump photon and stimulated emission of a Stokes photon gives rise to excitation of the QR. This scattering is described by the time-dependent Hamiltonian with matrix elements given by

$$\mathcal{H}_{n_r, m_\ell; n'_r, m'_\ell}(t) = -2\mathcal{V} \cos(\omega_{ps}t)\Theta(t)\Theta(\tau - t)\delta_{n_r, n'_r} \sum_{m=\pm 2L} \delta_{m_\ell, m'_\ell + m}, \quad (16)$$

where $\omega_{ps} = \omega_p - \omega_s$ is the difference of frequencies of the pump and Stokes pulses, and

$$\mathcal{V} = \frac{\mathcal{V}_e \mathcal{V}_b}{\hbar \Delta_{\text{hf}}}, \quad \mathcal{V}_b = \frac{g^2 \mu_B^2 B_p^{(0)} B_s^{(0)}}{3\hbar \Delta_{\text{hf}}}, \quad \mathcal{V}_e = \frac{4\alpha(\omega_e)}{\pi L!} \frac{P_e L^L e^{-L}}{w_e^2 c}, \quad (17)$$

P_e and w_e are the power and the beam waist of the optical pulse, $B_p^{(0)}$ and $B_s^{(0)}$ are the magnetic field strengths of the pump and Stokes radio-frequency pulses. The subscript e symbolizes the electric dipole interaction of the atom with the optical pulse, and the subscript b symbolizes the magnetic dipole interaction of the atoms with the pump and Stokes radio-frequency pulses. The detuning Δ_{hf} of the pump pulse frequency from the ${}^2S_{1/2}(F = 1/2) \rightarrow {}^2S_{1/2}(F = 1/2)$ quantum transition frequency greatly exceeds the frequency $\omega_{2L,0}$ of the $|0\rangle \rightarrow |2L\rangle$ quantum transition,

$$\Delta_{\text{hf}} \gg \omega_{2L,0}, \quad (18)$$

hence we can assume that ω_p and ω_s have the same detuning Δ_{hf} from resonance. Details of the Raman scattering of the pump and Stokes light, the Rabi oscillations with Raman pulses used to measure the energy differences of the QR states are presented Ref. [1] and also in the SM [14].

Consider the QR initially in the ground state $|0\rangle$ subjected to Raman pulses of duration τ and generalized Rabi frequency $\Omega_R = 2\sqrt{2}\mathcal{V}/\hbar$, such that $\Omega_R \tau \approx \pi$. In the 3-level rotating wave approximation [17], the temporal evolution of a single QR wave function is given by $|\Psi(\tau)\rangle = e^{-i\mathcal{H}_R \tau/\hbar}|0\rangle$, where \mathcal{H}_R is the Hamiltonian (see SM [14]),

$$\mathcal{H}_R = \hbar \begin{pmatrix} 0 & \Omega_R \sqrt{2}/4 & \Omega_R \sqrt{2}/4 \\ \Omega_R \sqrt{2}/4 & -\delta & 0 \\ \Omega_R \sqrt{2}/4 & 0 & -\delta \end{pmatrix}, \quad (19)$$

$\delta = \omega_{ps} - \omega_{2L,0}$, and the basis vectors are,

$$|0\rangle = \begin{pmatrix} 1 \\ 0 \\ 0 \end{pmatrix}, \quad |2L\rangle = \begin{pmatrix} 0 \\ 1 \\ 0 \end{pmatrix}, \quad |-2L\rangle = \begin{pmatrix} 0 \\ 0 \\ 1 \end{pmatrix}.$$

The probability of finding the quantum rotor in the final state $|f\rangle = 2^{-1/2}(|2L\rangle + |-2L\rangle)$ is

$$P_0(\delta, \Omega_R) = |\langle f|\Psi(\tau)\rangle|^2 = \frac{\Omega_R^2}{\Omega_R^2 + \delta^2} \sin^2\left(\frac{\tau}{2} \sqrt{\Omega_R^2 + \delta^2}\right). \quad (20)$$

$P_0(\delta, \Omega_R)$ has a peak, $P_0(0, \Omega_R) = 1$ at $\delta = 0$. The peak width at half maximum is $1.597 \Omega_R$.

When we have $N = 2j_{\max} + 1$ atoms singly occupying the sites with $|j| \leq j_{\max}$, the detuning of ω_{ps} from the resonant frequency of the j -th quantum rotor is $\delta_j = \delta + 4L^2 j^2 (\omega_0(r_l(0)) - \omega_0(r_l(z_j)))$, where δ is the detuning of ω_{ps} from the resonant frequency of the $j = 0$ QR, $\omega_0(r_l(z)) = \hbar/(2Mr_l^2(z))$ and $r_l(z_j)$ is the radius of the classical circular trajectory. As a result, the peak in the probability to find a QR in the final state is shifted and broadened. The probability to find a QR in the final state is

$$P(\delta, \Omega_R) = \frac{1}{2j_{\max} + 1} \sum_{j=-j_{\max}}^{j_{\max}} P_0(\delta_j, \Omega_R). \quad (21)$$

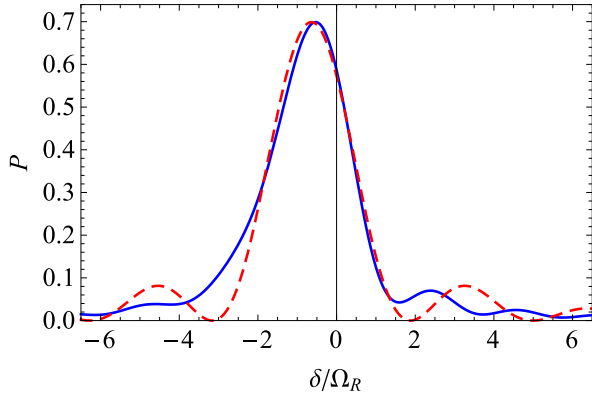


FIG. 4: The probability P in Eq. (21) for absorption of a pump photon and stimulated reemission of a Stokes photon with QRs quantum transition from state $|m_\ell = 0\rangle$ to $|m'_\ell = 50\rangle$ as a function of the difference $\omega_{ps} = \omega_p - \omega_s$ of the pump and Stokes frequencies ω_p and ω_s (solid blue curve). The dashed red curve shows the fit of $P(\delta, \Omega_R)$ obtained as explained in the text.

Figure 4 shows $P(\delta, \Omega_R)$ of Eq. (21) plotted as a function of δ , for $\omega_0 = 21.13 \text{ s}^{-1}$, which corresponds to a LG beam with $w_0 = 10 \mu\text{m}$ and $l = 25$, Rabi frequency $\Omega_R = 3.142 \text{ s}^{-1}$, pulse duration $\tau \approx \pi/\Omega_R = 1 \text{ s}$, $j_{\max} = 80$, $m_\ell = 0$ and $m'_\ell = 50$. The solid blue curve shows that $P(\delta, \Omega_R)$ has a peak, $P_{\max} = P(\delta_{\max}, \Omega_R) = 0.6989$, at $\delta_{\max} = -0.5374\Omega_R$. The dashed red curve shows the fitting of $P(\delta, \Omega_R)$ by the function $P(\delta, \Omega_R) \approx \mathcal{A} P_0(\delta - \delta_0, \tilde{\Omega}_R)$ with $\mathcal{A} = 0.67987$ and P_0 is given by Eq. (20) with $\delta_0 = -0.64002 \Omega_R$, $\tilde{\Omega}_R = 1.4865 \Omega_R$. Note

that $\delta_{\max} \neq \delta_0$. This is partly because the function $P(\delta, \Omega_R)$ is not symmetric with respect to the inversion $\delta - \delta_{\max} \rightarrow -(\delta - \delta_{\max})$, whereas the function $P_0(\delta, \Omega_R) = P_0(-\delta, \Omega_R)$ is symmetric.

We now show that ground-state QRs in an LG beam can serve as extremely accurate rotation sensors.

Rotation Sensor: Consider a QR in a non-inertial frame rotating with angular velocity $\mathbf{\Omega} = \Omega \mathbf{e}_z$ (see Fig. 2 in the SM [14]). The additional term needed in the Hamiltonian is

$$H_\Omega = \hbar\Omega\ell_z, \quad (22)$$

where $\ell_z = -i\partial_\phi$ is the orbital momentum operator. The Hamiltonian (22) lifts the symmetry under the transformation $(x, y, z) \rightarrow (-x, y, z)$ but not the rotational symmetry about the z -axis. As a result, m_ℓ , the eigenvalue of ℓ_z , is a good quantum number, and the energy levels ϵ_{m_ℓ} of the rotational motion become $\epsilon_{m_\ell}(\Omega) = \epsilon_{m_\ell} + \hbar\Omega m_\ell$. Hereafter we use the inequalities (15) and restrict ourselves by considering the quantum states with $n_z = n_r = 0$. Moreover, using the inequalities (15), we approximate the rotational energies as $\epsilon_{m_\ell} = m_\ell^2 C(r_l)$, where r_l is given by Eq. (6).

Let us consider the frequencies of the quantum transitions between the quantum states $|m_\ell\rangle$ and $|m'_\ell\rangle$ with $m_\ell = 0, \pm 1$ and $m'_\ell = m_\ell \pm 2L$. We have six spectral lines with frequencies $\omega_{m_\ell, m_\ell \pm 2L}(\Omega)$ which are convenient to order as follows: $\omega_{0, \pm 2L}(\Omega)$, $\omega_{\pm 1, \pm(1+2L)}(\Omega)$, and $\omega_{\pm 1, \pm(1-2L)}(\Omega)$. The frequencies of the quantum transitions between $|\zeta m_\ell\rangle$ and $|\zeta m_\ell + 2\zeta L\rangle$ are

$$\omega_{m_\ell, m_\ell + 2\zeta L}(\Omega) = 4L(L + m_\ell)\omega_0 + 2\zeta L\Omega. \quad (23)$$

where $\zeta = \pm 1$, and the rotational frequency is

$$\omega_0 = C(r_l)/\hbar. \quad (24)$$

Hence, when $\Omega = 0$, $\omega_{m_\ell, m_\ell + 2L}(0) = \omega_{-m_\ell, -(m_\ell + 2L)}(0)$. One can measure the three spectral lines $\omega_{0, 2L}(0) = \omega_{0, -2L}(0)$, $\omega_{1, 1-2L}(0) = \omega_{-1, -1+2L}(0)$, and $\omega_{1, 1+2L}(0) = \omega_{0, -1-2L}(0)$. When $\Omega \neq 0$, the degeneracy of the spectral lines is lifted and the splitting is

$$\Delta\omega_{m_\ell, m_\ell + 2L} \equiv \omega_{m_\ell, m_\ell + 2L}(\Omega) - \omega_{-m_\ell, -m_\ell - 2L}(\Omega) = 4L\Omega. \quad (25)$$

Eq. (25) shows that measuring the splitting of the spectral lines (23), can be used to determine Ω . Figure 5 shows the transition frequencies of the $|m_\ell\rangle \rightarrow |m_\ell \pm 50\rangle$ transitions as functions of Ω . The frequency splitting (25) due to Ω distinguishes between clockwise and counter-clockwise rotations. All the spectral lines have the same splittings. Hence, the frequencies satisfy the periodic condition,

$$\omega_{m_\ell + m_\Omega, m_\ell + m_\Omega + 2L}(\Omega - 2m_\Omega\omega_0) = \omega_{m_\ell, m_\ell + 2L}(\Omega),$$

where m_Ω is integer.

Rotation measurement accuracy estimate: Note that Eq. (25) does not contain any information regarding the optical potential, the laser frequency or the intensity. Therefore

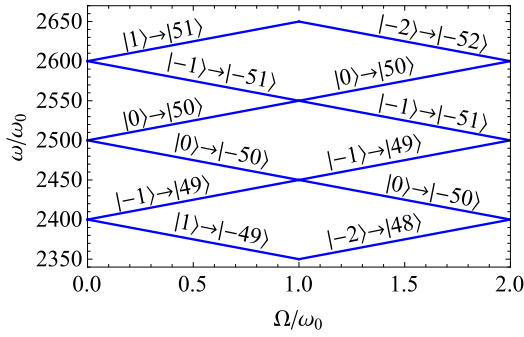


FIG. 5: The frequencies (23) of the quantum transitions $|m_\ell\rangle \rightarrow |m_\ell \pm 50\rangle$ versus the magnitude of the rotational velocity Ω . ω_0 is given by Eq. (24).

the uncertainty of Ω , $\delta\Omega$, is determined solely by uncertainty $\delta\omega$ of the pump and Stokes frequencies,

$$\delta\Omega = \frac{1}{\sqrt{N}} \frac{\delta\omega}{4L}. \quad (26)$$

Here $N = 2j_{\max} + 1$ is the number of atoms singly occupying the sites with $|j| \leq j_{\max}$, $\delta\omega = \delta\omega_p + \delta\omega_s$, and $\delta\omega_p$ and $\delta\omega_s$ are the uncertainties of the pump and Stokes frequencies. For ${}^6\text{Li}$ atoms, we take $\omega_p \gtrsim \omega_s \approx 1.43 \times 10^9 \text{ s}^{-1}$. $\delta\omega$ can be estimated as $\delta\omega = 2 \times 10^{-18} \omega_p \approx 2.86 \times 10^{-9} \text{ s}^{-1}$. From Eq. (26) we see that the larger L , the smaller is $\delta\Omega$; when $L = 25$ and $j_{\max} = 80$, $\delta\Omega = 2.25 \times 10^{-12} \text{ s}^{-1}$.

In order to measure angular velocity when gravity \mathbf{g} is present, place the QRs in the plane perpendicular to \mathbf{g} (let us call this the x - y plane), in order to measure the component of the angular velocity in the z direction. If an additional acceleration \mathbf{a} in the x - y plane is present, there is an additional splitting of the QR ground state degeneracy due to the acceleration, and the frequency splitting in Eq. (25) becomes dependent on m_ℓ . Hence, turn the plane of the QRs to be perpendicular to $\mathbf{g}' = \mathbf{g} - \mathbf{a}$ so that the frequency splitting (25) is independent on m_ℓ , and obtain the energy splitting of the levels caused just by $\Omega' = \boldsymbol{\Omega} \cdot \mathbf{e}'_z$, where \mathbf{e}'_z is the unit vector along $-\mathbf{g}'$. For details see the SM [14].

Summary and Conclusion: Cold atoms trapped in a Laguerre-Gauss optical potential (5) are confined to circular rings (donuts) of radius r_l with centers on the axis of the Laguerre-Gauss beam. Rings with one atom per site (to suppress spin-exchange collisions) can be used as high-accuracy rotation sensors. When $r_l = 15.81 \mu\text{m}$, the accuracy obtained

with $N = 161$ atoms singly occupying the sites with $|j| \leq 80$ is $\delta\Omega = 2.25 \times 10^{-12} \text{ s}^{-1}$. This is better than the accuracy $\delta\Omega = 6.4 \times 10^{-10} \text{ s}^{-1}$ reported in Ref. [1]. Moreover, the rotation sensor accuracy is much better than $\delta\Omega_{\text{NIST}} = 3 \times 10^{-8} \text{ s}^{-1}$ reported in Ref. [15].

The rings between the lenses in Fig. 1 have slightly different radii [see Eq. (6)]. As a result, different transition frequencies are obtained from of the $m_\ell \rightarrow m'_\ell$ transition for different z_j : $\omega_{m_\ell, m'_\ell}(z_j) = \omega_{m_\ell, m'_\ell}(0)C(r_l(z_j))/C(r_l(0))$. Hence, the width of the Rabi oscillation is broadened. For example, when $\omega_0 = 21.13 \text{ s}^{-1}$, $\Omega_R = 3.142 \text{ s}^{-1}$, and there are $N = 161$ singly occupied sites with $|j| \leq 80$, the resulting effective width of the Rabi oscillation peak is $\tilde{\Omega}_R = 1.4865 \Omega_R$ instead of Ω_R for a single QR (see Fig. 4).

This work was supported in part by a grant from the DFG through the DIP program (FO703/2-1).

-
- [1] I. Kuzmenko, T. Kuzmenko, Y. Avishai and Y. B. Band, Phys. Rev. A **100**, 033415 (2019).
 - [2] G. Goubau, and F. Scherwin, IRE Trans. **9**, 248256 (1961).
 - [3] L. Allen, *et al.*, Phys. Rev. A **45**, 8185 (1992).
 - [4] M.A. Clifford, J. Arlt, J. Courtial, K. Dholakia, Optics Communications **156**, 300 (1998).
 - [5] F. Pampaloni, Joerg Enderlein, arXiv:physics/0410021.
 - [6] W. H. Carter, M. F. Aburdene, J. Opt. Soc. Am. A **4**, 1949 (1987).
 - [7] L. Viverit, C. Menotti, T. Calarco, and A. Smerzi, Phys. Rev. Lett. **93**, 110401 (2004).
 - [8] I. Bloch, J. Dalibard, W. Zwerger, Rev. Mod. Phys. **80**, 885 (2008).
 - [9] J. M. Gibbons *et al*, Phys. Rev. A **78**, 043418 (2008).
 - [10] Alternatively, one could consider a different configuration consisting of a red-detuned version of a trap developed by T. Kuga *et al.*, Phys. Rev. Lett. **78**, 4713 (1997), with a LG beam and two additional ‘‘plugging’’ laser beams which limit the atomic motion along the optical axis of the LG beam.
 - [11] F. Le Kien, P. Schneeweiss and A. Rauschenbeutel, Eur. Phys. J. D **67**, 92 (2013).
 - [12] N. F. Ramsey, Phys. Rev. **78**, 695 (1950).
 - [13] T. Zanon-Willette *et al.*, Phys. Rev. A **90**, 053427 (2014).
 - [14] See supplemental materials, <http://xxx>.
 - [15] G.W. Hoth, B. Pelle, S. Riedl, J. Kitching, and E. Donley, Appl. Phys. Lett. **109**, 071113 (2016).
 - [16] Matevž Marinčič, ‘‘Cold atom gravimeter’’, University of Ljubljana, Ljubljana (2016). http://mafija.fmf.uni-lj.si/seminar/files/2015_2016/cold_at
 - [17] Y. Wu, X. Yang, Phys. Rev. Lett. **98**, 013601 (2007).

Supplemental Material for “Quantum Rotor Atoms in Light Beams with Orbital Angular Momentum: Highly Accurate Rotation and Acceleration Sensing”

Igor Kuzmenko^{1,4}, Tetyana Kuzmenko^{1,4}, Y. B. Band^{1,2,3,4}

¹*Department of Physics, Ben-Gurion University of the Negev, Beer-Sheva 84105, Israel*

²*Department of Chemistry, Ben-Gurion University of the Negev, Beer-Sheva 84105, Israel*

³*Department of Electro-Optics, Ben-Gurion University of the Negev, Beer-Sheva 84105, Israel*

⁴*The Ilse Katz Center for Nano-Science, Ben-Gurion University of the Negev, Beer-Sheva 84105, Israel*

Here we expand the discussion of the main text [1] as follows. Section I contains details regarding the Rabi oscillation method used to probe the energy levels of quantum rotors (QR) trapped in Laguerre-Gaussian (LG) beams to induce stimulated Raman transitions with radio-frequency pulses and optical frequency Laguerre-Gaussian pulses. Section II augments the analysis of the accuracy of the rotation sensor which uses QR atoms in LG beams, as proposed in [1]. Section III considers the discrimination against the effects of in-plane acceleration on the rotation sensor.

I. RABI OSCILLATIONS OF QUANTUM ROTOR STATES IN LG BEAMS

Here derive the time-dependent Hamiltonian in Eq. (16) of the main text [1] and treat the stimulated Raman process that gives rise to absorption of a pump photons and stimulated emission of Stokes photons thereby resulting in the excitation of the QRs.

Figure 3(a) of the main text [1] illustrates pump and Stokes radio-wave pulses (red and purple arrows) propagating in the x - y plane, and the optical LG pulses propagating along the z axis. The blue colors denote the depth of the optical pulse potential. The optical pulses lift the cylindrical symmetry of the trapping optical potential, Eq. (5) in [1], and allows quantum transitions with $\Delta m_\ell = \pm 2L$, i.e., it causes a rotational-kick to be applied to the QR. Figure 3(b) in [1] depicts quantum transitions between the ground state with $m_\ell = 0$ and excited states with $m'_\ell = \pm 2L$. The stimulated Raman scattering process is modeled using a time-dependent Hamiltonian with matrix elements given by Eq. (16) in the main text [1].

Consider Rabi oscillations resulting from the stimulated Raman process for the case when the low energy level is the $|m_\ell = 0\rangle$ state, the high-energy levels are $|m_\ell = \pm 2L\rangle$ states, and

$$\epsilon_{2L} = \epsilon_{-2L}, \quad \omega_{ps} = \frac{\epsilon_{2L} - \epsilon_0}{\hbar}.$$

The temporal evolution of the QR wave function, starting with the initial wave function $|0\rangle$, is specified by the time-dependent wave function

$$|\psi(t)\rangle = \cos\left(\frac{\Omega_R t}{2}\right) |0\rangle - \frac{i}{\sqrt{2}} \sin\left(\frac{\Omega_R t}{2}\right) \{|2L\rangle + |-2L\rangle\}, \quad (1)$$

where the Rabi frequency is

$$\Omega_R = \frac{2\sqrt{2}\mathcal{V}}{\hbar}. \quad (2)$$

Consider an alkali atoms in the ground $^2S_{1/2}$ state trapped in the Laguerre-Gaussian trapping potential (7) in the main text [1]. The atoms are illuminated by pump and Stokes radiofrequency waves far detuned by a detuning Δ_{hf} from the hyperfine splitting, and a laser beam far detuned from the excitation frequency of the $^2P_{3/2}$ state by a detuning Δ_e . Diagrams contributing to the quantum transitions $|0\rangle \rightarrow |\pm 2L\rangle$ in fourth-order perturbation theory are illustrated in Figs. 1(a) and 1(b). The frequencies of the pump and Stokes pulses are ω_p and ω_s , and the frequency of the laser pulse is ω_e . The detuning frequencies from the resonances are given by

$$\Delta_e = \omega_e - \omega(^2P_{3/2} - ^2S_{1/2}), \quad \Delta_{\text{hf}} = \omega_p - \omega_{\text{hf}} \gtrsim \omega_s - \omega_{\text{hf}}, \quad (3)$$

where $\omega(^2P_{3/2} - ^2S_{1/2})$ is a resonant frequency of the $^2S_{1/2} \rightarrow ^2P_{3/2}$ quantum transition, and ω_{hf} is the hyperfine splitting. We assume that

$$|\Delta_e| \gg |\Delta_{\text{hf}}| \gg \omega_{2L,0}, \quad (4)$$

where $\omega_{2L,0}$ is the frequency of the quantum transition $|0\rangle \rightarrow |2L\rangle$. Hence, we can neglect $\omega_{2L,0}$ compared with Δ_e , and take the same detuning Δ_e of ω_e from resonance with the $^2S_{1/2} \rightarrow ^2P_{3/2}$ transition [as shown in Figs. 1(a) and 1(b)]. Moreover, we assume that the detuning $\omega_p - \omega_{\text{hf}}$ of the pump pulse is approximately equal to the detuning $\omega_s - \omega_{\text{hf}}$ of the Stokes pulse.

Interactions of the trapped atom with the pump, Stokes and optical pulses are described by the Hamiltonians,

$$H_\mu = -g\mu_B \mathbf{s} \cdot \mathbf{B}_\mu(t), \quad H_e = -\mathbf{p} \cdot \mathbf{E}_e(\mathbf{r}, t), \quad (5)$$

where $\mu = p, s$ for the pump and Stokes pulses, \mathbf{s} is the spin-1/2 vector operator, and \mathbf{p} is the atomic electric dipole operator. The subscript e here and in Eq. (17) of [1] symbolizes the electric dipole interaction of the atom with the optical pulse, and the subscript b symbolizes the magnetic dipole interaction of the atoms with the pump and Stokes radio-frequency pulses. The electric field $\mathbf{E}_e(\mathbf{r}, t)$ and the magnetic field $\mathbf{B}_\mu(t)$ are given by

$$\mathbf{B}_\mu(t) = \mathbf{B}_\mu^{(0)} \cos(\omega_\mu t),$$

$$\mathbf{E}_e(\mathbf{r}, t) = \frac{1}{2} \{u_{L,0}(\mathbf{r}) + u_{-L,0}(\mathbf{r})\} \cos(k_e z) e^{-i\omega_e t} \mathbf{e}_x + \text{c.c.},$$

where $u_{L,0}(\mathbf{r})$ is given by Eq. (2) in the main text [1].

When a trapped atom absorbs and reemits an optical pulse photon, it gets a rotational-kicking quantum transition with $\Delta m_\ell = \pm 2L$, where m_ℓ is the orbital quantum number of orbital motion of the atom around the z axis, and L is the orbital

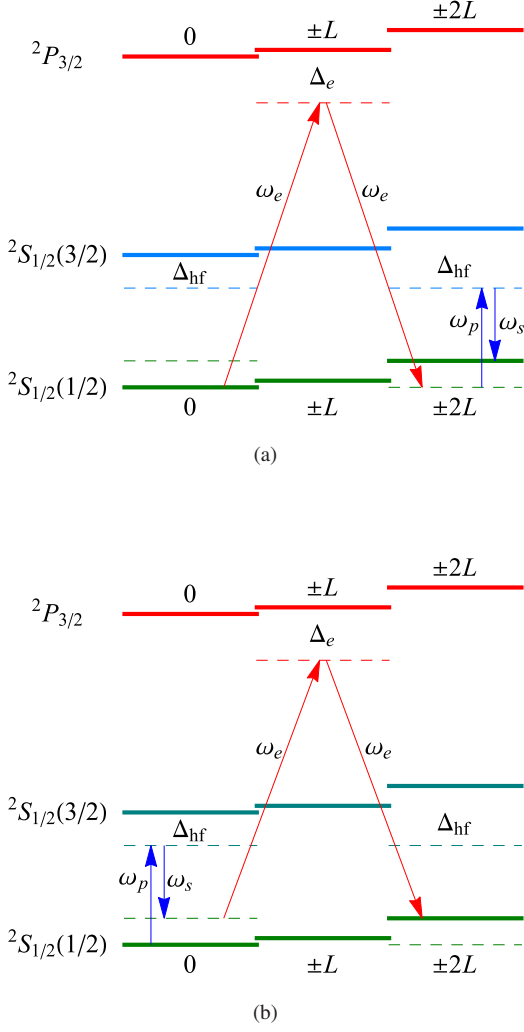


FIG. 1: Far-off resonance stimulated Raman scattering due to pump and Stokes radiofrequency waves (blue arrows) and optical rotation-kicking optical pulses (red arrows). The two diagrams of processes that contribute are shown. Δ_e is a detuning of ω_e from resonance with the ${}^2S_{1/2} \rightarrow {}^2P_{3/2}$ quantum transition, and Δ_{hf} is a detuning of ω_p from resonance of the ${}^2S_{1/2}(F=1/2) \rightarrow {}^2S_{1/2}(F=3/2)$ quantum transition. The detuning Δ_e and Δ_{hf} , and the frequency of the quantum transition $\omega_{2L,0} = (\epsilon_{2L} - \epsilon_0)/\hbar$ satisfy the inequalities (4), therefore the optical pulses are taken to have the same detuning Δ_e in both diagrams (a) and (b).

moment of the optical Laguerre-Gaussian (LG) pulse, see the main text [1] for details. From the other side, absorbing a pump photon and reemitting a Stokes photon, the atom gets the energy needed for quantum transitions. In this section, we apply fourth order perturbation theory and derive an effective Hamiltonian (16) in the main text [1]. This derivation is rather standard, but cumbersome.

We derive here an effective Hamiltonian describing Rabi oscillations for the QR in the $m_\ell = 0$ and $\pm 2L$ states. For this purpose, we assume that the low-energy states of the

trapped atom are $|{}^2S_{1/2}(1/2), m_\ell, m_F\rangle$ states with the electronic configuration ${}^2S_{1/2}(F=1/2)$, magnetic quantum number $m_F = \pm 1/2$ and the motion of the center of mass parametrized by $m_\ell = 0, \pm 2L$. High-energy states are $|{}^2S_{1/2}(3/2), m_\ell, m_F\rangle$ with electronic configuration ${}^2S_{1/2}(F=3/2)$, $m_\ell = 0, \pm 2L$ and $m_F = \pm 1/2$, and $|{}^2P_{3/2}, m_\ell, m_F\rangle$ with electronic configuration ${}^2P_{3/2}$, $m_\ell = \pm L$ and $m_F = \pm 1/2$, as illustrated in Fig. 1. In this section, we use the following basis,

$$|0\rangle = |{}^2S_{1/2}(1/2), 0, m_F\rangle, \quad (6a)$$

$$|1\rangle = \frac{1}{\sqrt{2}} \left\{ |{}^2S_{1/2}(1/2), 2L, m_F\rangle + |{}^2S_{1/2}(1/2), -2L, m_F\rangle \right\}, \quad (6b)$$

$$|2\rangle = e^{i\omega_p t} |{}^2S_{1/2}(3/2), 0, m_F\rangle, \quad (6c)$$

$$|3\rangle = \frac{e^{i\omega_p t}}{\sqrt{2}} \left\{ |{}^2S_{1/2}(3/2), 2L, m_F\rangle + |{}^2S_{1/2}(3/2), -2L, m_F\rangle \right\}, \quad (6d)$$

$$|4\rangle = \frac{e^{i\omega_e t}}{\sqrt{2}} \left\{ |{}^2P_{3/2}, L, m_F\rangle + |{}^2P_{3/2}, -L, m_F\rangle \right\}. \quad (6e)$$

The “non-perturbed” Hamiltonian of the trapped atom without the pump, Stokes and optical pulses is given by the matrix elements,

$$\langle v|H_0|v'\rangle = \epsilon_v \delta_{v,v'}, \quad (7)$$

where

$$\epsilon_0 = 0, \quad \epsilon_1 = \epsilon_{2L}, \quad \epsilon_2 = \hbar\Delta_{\text{hf}}, \quad \epsilon_3 = \hbar\Delta_{\text{hf}} + \epsilon_{2L}, \quad \epsilon_4 = \hbar\Delta_e.$$

The energy of the rotational motion of the atom is $\epsilon_{m_\ell} = m_\ell^2 C(r_l)$, where $C(r_l) = \hbar^2/(2Mr_l^2)$ and r_l is the radius of the classical circular trajectory. $\Delta_{\text{hf}} = \omega_p - \epsilon_{\text{hf}}/\hbar$ and $\Delta_e = \omega_e - \epsilon_e/\hbar$ are the detuning of the pump and optical frequencies from the resonant frequencies of the quantum transitions $|0\rangle \rightarrow |3\rangle$ and $|0\rangle \rightarrow |4\rangle$, respectively.

Nontrivial matrix elements of H_p , H_s and H_e , Eq. (5), are

$$\begin{aligned} \langle 1|H_\mu|3\rangle &= \langle 2|H_\mu|4\rangle = g\mu_B B_\mu \langle 1/2, m_F|s_x|3/2, m_F\rangle \\ &= \frac{\sqrt{2}}{3} g\mu_B B_\mu e^{i(\omega_\mu - \omega_p)t} m_F, \end{aligned} \quad (8a)$$

$$\begin{aligned} \langle 1|H_e|5\rangle &= \langle 2|H_e|5\rangle = \frac{1}{2} [u_{L,0}(r_l, 0, 0) + u_{-L,0}(r_l, 0, 0)] \\ &\quad \times \langle {}^2S_{1/2}, m_F|p_x|{}^2P_{3/2}, m_F\rangle, \end{aligned} \quad (8b)$$

where $u_{L,0}(r, \phi, z)$ are given by Eq. (2) in the main text [1]. Here we chose the x axis as a quantization axis.

A. Adiabatic elimination of the ${}^2S_{1/2}(F=3/2)$ hyperfine state

As a first step, we apply the following unitary transformations,

$$\begin{aligned} |\psi_0\rangle &= u_b|0\rangle - v_b|2\rangle, & |\psi_1\rangle &= u_b|1\rangle - v_b|3\rangle, \\ |\psi_2\rangle &= v_b^*|0\rangle + u_b|2\rangle, & |\psi_3\rangle &= v_b^*|1\rangle + v_b|3\rangle, \end{aligned}$$

and $|\psi_4\rangle = |4\rangle$, where

$$v_b = \frac{\sqrt{2}}{3} \frac{g\mu_B(B_p + B_s e^{-i\omega_{ps}})}{\hbar\Delta_{\text{hf}}}, \quad u_b = \sqrt{1 - |v_b|^2}, \quad (9)$$

and $\omega_{ps} = \omega_p - \omega_s$. We assume here that $|v_b| \ll 1$ and keep terms up to v_b^2 , and neglect v_b^n with $n \geq 3$. This transformation makes $H_0 + H_p + H_s$ diagonal,

$$\langle \psi_n | H_0 + H_p + H_s | \psi_{n'} \rangle = \tilde{\epsilon}_n \delta_{n,n'},$$

where

$$\begin{aligned} \tilde{\epsilon}_0 &= -\Delta_{\text{hf}}|v_b|^2, \\ \tilde{\epsilon}_1 &= \epsilon_{2L} - \Delta_{\text{hf}}|v_b|^2, \\ \tilde{\epsilon}_2 &= \Delta_{\text{hf}}(1 + |v_b|^2), \\ \tilde{\epsilon}_3 &= \epsilon_{2L} + \Delta_{\text{hf}}(1 + |v_b|^2), \\ \tilde{\epsilon}_4 &= \tilde{\epsilon}_4. \end{aligned}$$

Matrix elements of H_e are

$$\begin{aligned} h_e &\equiv \langle \psi_0 | H_e | \psi_4 \rangle = \langle \psi_1 | H_e | \psi_4 \rangle \\ &= \frac{1}{2} [u_{L,0}(r_l, 0, 0) + u_{-L,0}(r_l, 0, 0)] \times \\ &\quad \langle {}^2S_{1/2}, m_F | p_x | {}^2P_{3/2}, m_F \rangle \left(1 - \frac{|v_b|^2}{2}\right), \end{aligned} \quad (10)$$

where $u_{L,0}(r, \phi, z)$ is given by Eq. (2) in the main text [1].

B. Adiabatic elimination of the ${}^2P_{3/2}$ excited state

In a second step, we apply the following unitary transformations,

$$\begin{aligned} |\tilde{\psi}_0\rangle &= u_g |\psi_0\rangle - \frac{v_e^2}{2} |\psi_1\rangle - v_e |\psi_4\rangle, \\ |\tilde{\psi}_1\rangle &= -\frac{v_e^2}{2} |\psi_0\rangle + u_g |\psi_1\rangle - v_e |\psi_4\rangle, \\ |\tilde{\psi}_4\rangle &= v_e |\psi_0\rangle + v_e |\psi_1\rangle + u_e |\psi_4\rangle, \end{aligned}$$

where

$$v_e = \frac{h_e}{\Delta_e}, \quad u_g = \sqrt{1 - |v_e|^2}, \quad u_e = \sqrt{1 - 2|v_e|^2}.$$

We assume here that $|v_e| \ll 1$ and keep terms up to v_e^2 and neglect terms proportional to v_e^n with $n \geq 3$. Then the transformed Hamiltonian $H = H_0 + H_p + H_s + H_e$ is given by the matrix elements,

$$\begin{aligned} \langle \tilde{\psi}_n | H | \tilde{\psi}_{n'} \rangle &= \tilde{\epsilon}_n \delta_{n,n'} - \frac{2|h_e|^2}{\Delta_e}, \\ \langle \tilde{\psi}_4 | H | \tilde{\psi}_4 \rangle &= \Delta_e + \frac{4|h_e|^2}{\Delta_e}, \\ \langle \tilde{\psi}_n | H | \tilde{\psi}_4 \rangle &= 0, \end{aligned}$$

where $n, n' = 0, 1$.

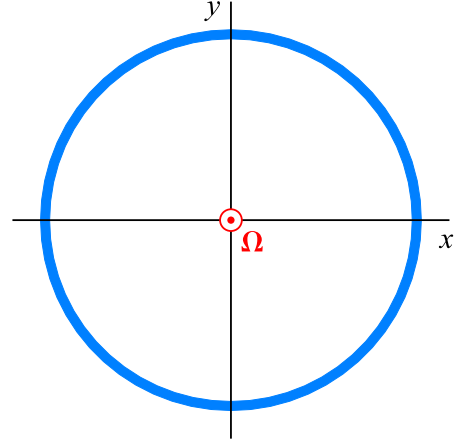


FIG. 2: QR (blue ellipse) subject to a rotation with angular velocity $\mathbf{\Omega} = \Omega_e \mathbf{e}_z$.

Omitting the high-energy state $|\tilde{\psi}_4\rangle$, we get the two-level effective Hamiltonian describing Rabi oscillations,

$$H = \begin{pmatrix} 0 & -2|h_e|^2/\Delta_e \\ -2|h_e|^2/\Delta_e & \epsilon_{2L} \end{pmatrix}, \quad (11)$$

where we shift the chemical potential by adding the term

$$\left(\Delta_{\text{hf}}|v_b|^2 + \frac{2|h_e|^2}{\Delta_e}\right) \begin{pmatrix} 1 & 0 \\ 0 & 1 \end{pmatrix}.$$

Taking into account Eqs. (10) and (9), we get

$$\begin{aligned} \frac{2|h_e|^2}{\Delta_e} &= \frac{\alpha(\omega_e)}{2} |u_{L,0}(r_l, 0, 0) + u_{-L,0}(r_l, 0, 0)|^2 \times \\ &\quad \left\{1 - \frac{1}{3} \frac{g^2 \mu_B^2}{\hbar^2 \Delta_{\text{hf}}^2} [B_p^2 + B_s^2 + 2B_p B_s \cos(\omega_{ps}t)]\right\}. \end{aligned} \quad (12)$$

On the right hand side of Eq. (12) there are time-independent and time-dependent terms. The former can be considered as weak perturbation which does not contribute to the Rabi oscillations, whereas the second term gives rise to Rabi oscillations. Off-diagonal part of the Hamiltonian (11) after omitting the time-independent terms gives us the Rabi oscillation Hamiltonian (16) in the main text [1].

II. ROTATION SENSOR ACCURACY

When QRs are placed in a non-inertial frame rotating with angular velocity $\mathbf{\Omega} = \Omega_e \mathbf{e}_z$ (as described in the main text [1] and as illustrated in Fig. 2), they can be used as a high accuracy rotation sensor to determine Ω . The accuracy of the rotation sensor due to uncertainty of the pump and Stokes frequencies is analyzed in the main text. Here we derive the uncertainty in the angular velocity due to Rabi frequency fluctuations and due to shot noise in the pump and Stokes pulses.

A. Uncertainty due to Rabi frequency fluctuation

The energies $\epsilon_{m_\ell} = m_\ell^2 C(r_l)$ do not depend on the laser frequency and intensity. Therefore, the frequencies of the quantum transitions $|m_\ell\rangle \rightarrow |m'_\ell\rangle$ are independent of the laser frequency and intensity. Hence, the only source of uncertainty is fluctuations in frequencies of the Stokes, pump and “kick” pulses which results in fluctuations in the Rabi oscillations. Indeed, fluctuations of frequencies result in fluctuations in the Rabi frequency (2),

$$\phi_R = \Omega_R \tau_\pi = \pi \pm \delta\phi_\omega, \quad (13)$$

where

$$\begin{aligned} \delta\phi_\omega &= \sqrt{\sum_{\kappa=p,s} \left(\frac{\partial\phi_R}{\partial\omega_\kappa} \delta\omega_\kappa \right)^2} \\ &= \phi_R \sqrt{\left(\frac{\delta\omega_p}{\Delta_{\text{hf}}} \right)^2 + \left(\frac{\delta\omega_s}{\Delta_{\text{hf}}} \right)^2}. \end{aligned} \quad (14)$$

Taking $\delta\omega_p \approx \delta\omega_s = 2.86 \times 10^{-9} \text{ s}^{-1}$ (see the main text [1]) and $\Delta_{\text{hf}} = 1.26 \times 10^8 \text{ s}^{-1}$, we get

$$\frac{\delta\phi_\omega}{\phi_R} = 3.21 \times 10^{-17}. \quad (15)$$

When the energy levels $\epsilon_{\pm 2L}$ are not degenerate, but $\Delta\epsilon = \epsilon_{2L} - \epsilon_{-2L}$ is small in comparison to $\epsilon_{2L} - \epsilon_0$, the difference $\Delta\phi_\epsilon \equiv \phi_{2L} - \phi_{-2L}$ is

$$\Delta\phi_\epsilon = \frac{\Delta\epsilon}{4\hbar\Omega_R}, \quad (16)$$

where Ω_R is the Rabi frequency (2). The levels $\epsilon_{\pm 2L}$ can be distinguished when $\Delta\phi_\epsilon > \delta\phi_\omega$, or

$$\frac{\Delta\epsilon}{C(r_l)} > \frac{\delta\epsilon_\omega}{C(r_l)} = \frac{4\hbar\Omega_R}{C(r_l)} \delta\phi_\omega = 5.998 \times 10^{-17}, \quad (17)$$

where we take $\Omega_R = 3.142 \text{ s}^{-1}$. Then, taking $C(r_l) = k_B \times 0.1613 \text{ nK}$ (which corresponds to the Laguerre-Gaussian beam with $l = 5$, $p = 0$ and $w_0 = 10 \mu\text{m}$, see Eq. (2) in the main text [1]), we get the uncertainty of the energy splitting $\delta\epsilon_\omega$ as

$$\delta\epsilon_\omega = \hbar \times 1.267 \times 10^{-15} \text{ s}^{-1}. \quad (18)$$

Knowing the uncertainty $\delta\epsilon_\omega$ of the energy splitting, we are able to estimate the uncertainty $\delta\Omega_\omega$ of the rotation sensor,

$$\delta\Omega_\omega = \frac{1}{\sqrt{N}} \frac{\delta\epsilon_\omega}{4L\hbar}, \quad (19)$$

where $N = 2j_{\text{max}} + 1$ is the number of singly-occupied rings filled with QR atoms. When $L = 25$ and $N = 161$, then

$$\delta\Omega_\omega = 9.985 \times 10^{-19} \text{ s}^{-1}.$$

Comparing this result with $\delta\Omega$ in Eq. (23) in the main text [1], one can see that uncertainty in Ω due to fluctuations of the Rabi frequency is very small with respect to the uncertainty $\delta\Omega$ due to the fluctuations of the pump and Stokes frequencies.

B. Uncertainty due to shot noise in the pump and Stokes pulses

Another source of uncertainty arises from shot noise in the Stokes, pump and kick pulses. Shot noise results in fluctuations in the position and amplitude of the population oscillations of the Ramsey fringes because of fluctuation of the Rabi frequencies,

$$\phi_R = \Omega_R \tau_\pi = \pi \pm \delta\phi_I, \quad (20)$$

where

$$\delta\phi_I \approx \pi \left(\frac{1}{\sqrt{N_p}} + \frac{1}{\sqrt{N_s}} \right), \quad (21)$$

where N_p and N_s are the number of photons in the pump and Stokes pulses during the time $\tau_\pi = \pi/\Omega_R$. When $N_p \sim N_s \sim 10^{29}$, then

$$\delta\phi_I = 1.987 \times 10^{-14}.$$

Uncertainty in the energy splitting can be estimated in a fashion similar to Eq. (17),

$$\frac{\Delta\epsilon}{4\hbar\Omega_R} > \frac{\delta\epsilon_I}{4\hbar\Omega_R} = \frac{\delta\phi_I}{\phi_R} = 6.325 \times 10^{-15}. \quad (22)$$

For $\Omega_R = 3.142 \text{ s}^{-1}$, we get $\delta\epsilon_I = \hbar \times 7.949 \times 10^{-14} \text{ s}^{-1}$.

Knowing the uncertainty $\delta\epsilon_I$ of the energy splitting, we are able to estimate the uncertainty $\delta\Omega_I$ of the rotation sensor,

$$\delta\Omega_I = \frac{1}{\sqrt{N}} \frac{\delta\epsilon_I}{4L\hbar}, \quad (23)$$

where $N = 2j_{\text{max}} + 1$ is the number of singly-occupied rings filled with QR atoms. When $L = 25$ and $N = 161$, the uncertainty is

$$\delta\Omega_I = 6.265 \times 10^{-17} \text{ s}^{-1}.$$

Comparing these results with Eq. (23) in the main text [1], one can see that the uncertainty in Ω due to shot noise in the pump, Stokes and kick pulses is of the same order of magnitude as the uncertainties due to fluctuations the pump and Stokes frequencies.

III. DISCRIMINATING AGAINST IN-PLANE ACCELERATION

An additional term $H_g = -\mathbf{M}\mathbf{g} \cdot \mathbf{r}$ must be added into the QR Hamiltonian to model the affects of a gravitational field \mathbf{g} [2]. This preserves the rotational symmetry in the plane perpendicular to \mathbf{g} (the x - y plane in Fig. 3), but lifts the rotational symmetry in the x - z and y - z planes. As a result, the QRs rotating in the x - y plane clockwise and counterclockwise with the same quantum number $|m_\ell\rangle$ have the same energy. When the QRs are placed in the x - z or y - z plane (such that \mathbf{g} is in the plane of the QRs), the degeneracy of the quantum states $|m_\ell\rangle$ and $| -m_\ell\rangle$ are split and the splitting depends on m_ℓ . Hence,

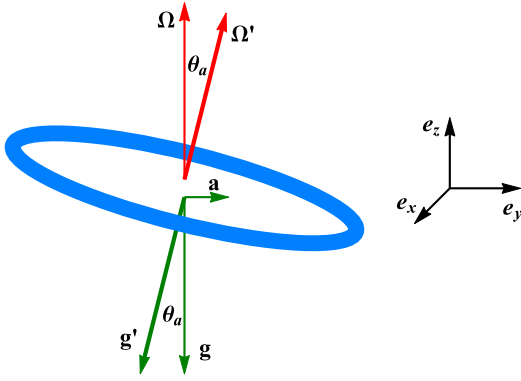


FIG. 3: Elimination of the in-plane acceleration \mathbf{a} by inclining the QRs. Here $\mathbf{g} = -g\mathbf{e}_z$ is the acceleration due to gravity, $\mathbf{\Omega}$ is the angular velocity, and $\mathbf{g}' = \mathbf{g} - \mathbf{a}$ is the total acceleration, where \mathbf{e}_x , \mathbf{e}_y and \mathbf{e}_z are unit vectors parallel to the x -, y - and z -axes. $\mathbf{\Omega}' = \Omega'\mathbf{e}'_z$, where $\Omega' = (\mathbf{\Omega} \cdot \mathbf{e}'_z)$ and the unit vector \mathbf{e}'_z is antiparallel to \mathbf{g}' . The angle between \mathbf{g} and \mathbf{g}' is θ_a . Blue ellipse is the QR placed in the plane perpendicular to \mathbf{g}' .

placing the QRs in the x - y plane, we obtain the energy splitting of the levels caused just by Ω_z (the z component of the angular velocity $\mathbf{\Omega}$).

Now consider QRs placed in a non-inertial frame moving with acceleration \mathbf{a} . The effective gravity \mathbf{g}' in the non-inertial frame is given by $\mathbf{g}' = \mathbf{g} - \mathbf{a}$. Therefore, when we turn the QRs to the plane perpendicular to \mathbf{g}' , we obtain the splitting of the energy levels caused just by $\Omega' = \mathbf{\Omega} \cdot \mathbf{e}'_z$, as illustrated in Fig. 3, where \mathbf{e}'_z is the unit vector along $-\mathbf{g}'$.

[1] I. Kuzmenko, T. Kuzmenko, Y. B. Band, “Quantum Rotor Atoms in Light Beams with Orbital Angular Momentum: Highly Accurate Rotation and Acceleration Sensing”, to be published.

[2] I. Kuzmenko, T. Kuzmenko, Y. Avishai and Y. B. Band, Phys. Rev. A **100**, 033415 (2019).